COUPLING BETWEEN THE BACTERIORHODOPSIN PHOTOCYCLE AND THE PROTONMOTIVE FORCE IN *HALOBACTERIUM HALOBIUM* CELL ENVELOPE VESICLES

II. Quantitation and Preliminary Modeling of the M → bR Reactions

G. I. GROMA, S. L. HELGERSON, P. K. WOLBER, D. BEECE, ZS. DANCSHÁZY, L. KESZTHELYI, AND W. STOECKENIUS

Department of Biochemistry and Biophysics and Cardiovascular Research Institute, University of California, San Francisco, California 94143

ABSTRACT The cell membrane of *Halobacterium halobium* (*H. halobium*) contains the proton-pump bacteriorhodopsin, which generates a light-driven transmembrane protonmotive force. The interaction of the bacteriorhodopsin photocycle with the electric potential component of the protonmotive force has been investigated. *H. halobium* cell envelope vesicles have been prepared by sonication and further purified by ultracentrifugation on Ficoll/NaCl/CsCl density gradients. Under continuous illumination (550 ± 50 nm) varied from 0 to 40 mW cm^{-2}, the vesicles maintain a membrane potential of 0 to −100 mV. The membrane potential was measured by flow dialysis of ^{3}H-TPMP$^+$ uptake and could be abolished by the uncoupler carbonylcyanide-*m*-chlorophenylhydrazone. Time-resolved absorption spectroscopy was used to measure the decay kinetics of the M photocycle intermediate, which was initiated by a weak laser flash (588 nm), while the vesicles were continuously illuminated as above. The M decay kinetics were fitted with two exponential decays by a computer deconvolution program. The faster decaying form decreases in amplitude (70 to 10% of the total) and the slower decaying form increases in amplitude and lifetime (23 to 42 ms) as the background light intensity increases. Although any correlation between the membrane potential and the bacteriorhodopsin photocycle M-forms is complex, the present data will allow specific tests of the physical mechanism for this interaction to be designed and conducted.

INTRODUCTION

Bacteriorhodopsin (bR) occurs in the cell membrane of *Halobacterium halobium* (*H. halobium*) in the form of crystalline patches, known as purple membrane (pm). It acts in vivo as a light energy-converting electrogenic proton pump that generates a transmembrane electric potential and a pH gradient. The resulting protonmotive force (pmf) is utilized by the cell to drive ATP synthesis, ion movements, and metabolite transport. For a review see reference 1. Heinz has shown that the generated ionmotive force should affect the kinetics of an electrogenic ion pump (2). In a previous paper (3) we studied the bR photocycle in *H. halobium* cells and found that under physiological conditions, the photocycle in the intact cell can markedly differ from that of isolated purple membrane. Under the conditions tested, the decay of the M photocycle intermediate could be correlated qualitatively with the transmembrane electric potential ($\Delta\Psi$). It has recently been suggested (4) that two pathways may exist for the regeneration of bR. Only one pathway leads to proton pumping while the nonpumping pathway becomes more probable at high $\Delta\Psi$. Similar conclusions have been reported (5). The present work establishes a more quantitative relationship between the kinetics of M-like forms and $\Delta\Psi$. We used cell envelope vesicles in this study instead of intact cells because the main effects are less disturbed by additional physiological reactions. Also, the steady state membrane potential can be easily generated and varied by continuous illumination, no membrane potential exists in the dark, the light scattering of the sample is lower, and the samples are more stable.

MATERIALS AND METHODS

Preparation and Characterization of Cell Envelope Vesicles

H. halobium strain JW-3 (kindly provided by H. J. Weber) (6, 7) was grown in 12-l fermentors as described previously (8). The cells were

Dr. Groma's, Dr. Dancsházy's, and Dr. Keszthelyi's permanent address is the Institute of Biophysics, Biological Research Center, Hungarian Academy of Sciences, H-6701 Szeged, Hungary.

Dr. Beece's permanent address is the Department of Physics, University of Illinois, Urbana, Illinois 61801.

harvested after 4 to 6 days' growth, washed two or three times with basal salts (BS, 4 M NaCl, 33 mM KCl, 81 mM $MgSO_4$) containing DNase, and once with BS. Then the cells were washed and resuspended to 1/35 the original volume in 4 M NaCl + 50 mM Tris (pH 7.0; Sigma Chemical Corp., St. Louis, MO). The cell suspension was sonicated in 30-ml portions six times for 15 s and kept on ice for at least 30 s between sonications. A sonicator (W-350; Branson Sonic Power Co., Danbury, CT) with a standard microtip was used at the following settings: continuous output, output control 4–5, output 150 W. After sonication the crude cell envelope vesicle fraction was isolated as described by Lanyi and MacDonald (9).

The crude cell envelope vesicle preparation was further fractionated by ultracentrifugation on Ficoll-400/CsCl/NaCl density step gradients. The crude vesicle suspension in 4 M NaCl was layered on step gradients prepared by standard techniques. From top to bottom the steps were 4% Ficoll at $\rho = 1.17$ g ml^{-1}, 8% Ficoll at $\rho = 1.195$ g ml^{-1}, 25% Ficoll at $\rho >$ 1.20 g ml^{-1}, where the Ficoll was dissolved in 4 M NaCl and the indicated density achieved by addition of CsCl. The gradients were centrifuged for 45 min at 22,500 rpm and 10°C in a VTi50 vertical rotor (L8-80 Ultracentrifuge; Beckman Instruments Inc., Fullerton, CA). The right-side out vesicles banded at the 4–8% interface, while the nonvesicular purple membrane banded at the 8–25% interface. The material at each interface was collected, washed 2 to 3 times, and resuspended at ~1 mg protein ml^{-1} in 4 M NaCl. For each membrane fraction the protein and bacteriorhodopsin contents were determined using the Lowry assay and the light-dark adaptation assay (10), respectively. The orientation and intactness were monitored with the menadione reductase-NADH assay (11). The internal water-permeable space was measured using ^3H_2O and (^{14}C)-sucrose as described by Bakker et al. (12). To minimize the development of ionic gradients during illumination, the vesicles were loaded by osmotic shock and resuspended at ~5 mg protein ml^{-1} with either 3 M NaCl or 3 M KCl in 50 mM HEPES buffer (pH 7.6). Steady state membrane potential was measured using flow dialysis of (^{3}H)-$TPMP^+$ as described previously (13). The actinic illumination was provided by the same Xe lamp and optical filters used in the spectroscopic measurements (see below).

Time-resolved Absorbance Changes

We used an instrument similar to that described previously (3). The beam from a 100 W tungsten-iodide lamp was defined by a monochromator (415 nm if not otherwise indicated) and focused onto a thermostated (20°C) 2 × 2 mm optical pathlength rectangular cuvette containing the sample. The transmitted light was monitored by an EMI 9558A photomultiplier tube (EMI Gencom Inc., Plainview, NY) protected by bandpass or interference filters from the actinic laser flash, which initiated the photoreaction cycle.

To generate and control the steady state membrane potential, the vesicles were illuminated with a continuous background light. The light of a 500 W high-pressure Xe lamp was heat-filtered, passed through a high-pass glass filter (3-70; Corning Glass Works, Corning Medical and Scientific, Corning, NY) and an interference filter (550 nm, half-width = 50 nm; BB5500 20992CC; Corion Corp., Holliston, MA), and focused onto a light pipe. Its intensity was controlled by a set of neutral density filters. This light illuminated the cuvette at a right angle to the monitoring beam. The light intensity without any neutral filter was 40 mW cm^{-2} in the plane at the middle of the cuvette holder.

The actinic flash from a dye laser (588 nm; Molectron Corp., Sunnyvale, CA) reached the sample through a light pipe at a right angle to the monitoring beam. 16 flashes were averaged with 10-s dark periods allowing the sample to relax completely after every flash (3). We observed previously an intensity dependence of the photocycle kinetics for high intensity single flashes. To prevent this effect, the laser intensity was reduced until no further change in the M decay kinetics was observed when the intensity was reduced an additional tenfold. The intensity of the monitoring beam was checked for actinic effects in the same way. Both intensities were then kept at appropriately low levels during the experiment.

The photomultiplier tube output was amplified using a current amplifier with a rise time of 0.3 ms (model 427; Keithley Instruments Inc., Cleveland, OH) and stored using a Nicolet 1180 computer (4K points, dwell time/pt = 50 μs; Nicolet Instrument Corp., Madison, WI). The data were analyzed by converting the transmission changes to absorbance changes and fitting with exponential decays using a modified variation of the VARP program.

RESULTS

Fractionating the crude cell envelope vesicle preparation using Ficoll/CsCl/NaCl density gradient centrifugation is the important prerequisite to the spectroscopic experiments described below. *H. halobium*, strain JW-3, is a bR overproducer with minimal carotenoid content. Thus, it is well suited for spectroscopic examination of the bR photocycle in vivo. However, during vesicle preparation from this strain, large amounts of nonvesicular, aggregated purple membrane fragments are produced. The Ficoll/CsCl/NaCl step gradient effectively separates this nonvesicular fraction from the closed, right-side out vesicles. The ratio of vesicular to nonvesicular fraction protein contents in the crude preparation is 2 or 3 to 1 (observed in five preparations, data not shown). As shown below, only bR present in energetically closed membrane vesicles and subjected to a transmembrane electric potential, $\Delta\Psi$, displays the slowing

TABLE I
INTERNAL VOLUME, MENADIONE REDUCTASE ACTIVITY AND BACTERIORHODOPSIN CONTENT OF *H. HALOBIUM* CELL ENVELOPE VESICLES AND THE NONVESICULAR MEMBRANE FRACTION

Sample fraction*	Internal volume (IV)			
	Pellet protein	Pellet water	α§	IV
	mg	*μl/mg*		*μl/mg*
Vesicular‡	0.07	14.4	0.59	8.5
	0.16	16.2	0.54	8.8
Nonvesicular	0.12	13.0	0.02	0.3

	Menadione reductase (MDR) activity (nmol NADH/mg/min)		
	Protein	MDR (−Triton)	MDR (+Triton)
	mg/ml		
Vesicular	0.30	2.1	20.4
Nonvesicular	0.29	—	2.2

	Bacteriorhodopsin (bR)		
	Protein	ΔOD_{590}^{LA-DA}	bR
	mg/ml		*nmol/mg* protein
Vesicular	0.66	0.041	5.2
Nonvesicular	0.61	0.050	6.9

*All samples loaded and suspended in 3 M NaCl.
‡Two separate determinations of internal volume are shown.
§α is the fraction of the pellet that is internal water space (12).

down in the photocycle kinetics described previously (3). Nonvesicular purple membrane would contribute a large background to the spectroscopic signals and make interpretation of the data difficult.

The measured internal volume, menadione reductase activity, and bR content of a vesicular and a nonvesicular fraction are shown in Table I. The nonvesicular fraction shows essentially no internal volume, while the vesicles have ~9 μl internal water space per milligram protein. Menadione reductase activity measured before and after lysing the vesicles with Triton X-100 indicates that the vesicles are right-side out and at least 90% intact. Other preparations ranged from 90 to 95% intact. After Triton treatment the nonvesicular fraction consistently showed <10% of the menadione reductase-specific activity seen in the vesicular fraction. Their bR content is similar, although the nonvesicular fraction is usually somewhat enriched in this protein.

Flow dialysis with ^{3}H-TPMP$^+$ accurately measures $\Delta\Psi$ in *H. halobium* cell envelope vesicles (13). As shown here in Fig. 1 *A* and *C*, the membrane potential maintained by the vesicles is a function of the actinic light intensity and can be completely collapsed by the uncoupler CCCP. The experiments were performed at pH 7.6 with a high internal and external buffer concentration so that the vesicles do not develop a steady state transmembrane pH gradient (data not shown) (13). The nonvesicular fraction shows no measurable light-induced membrane potential under the same conditions (Fig. 1 *B*).

In agreement with previous work on whole cells (3), continuous illumination, which generates $\Delta\Psi$, slows down the kinetics of the M decay in vesicle preparations (Fig. 2), when measured by the half decay time of the M_{415} intermediate ($t_{1/2}$). In the case of NaCl vesicles at low continuous light intensities $t_{1/2}$ increases rapidly with the light intensity, but at higher intensities $t_{1/2}$ decreases slightly. KCl vesicles behave similarly, but the changes in $t_{1/2}$ are not as large (Fig. 3). This is to be expected because vesicles loaded with and suspended in NaCl develop approximately twice the $\Delta\Psi$ found if KCl is present (13). As expected in

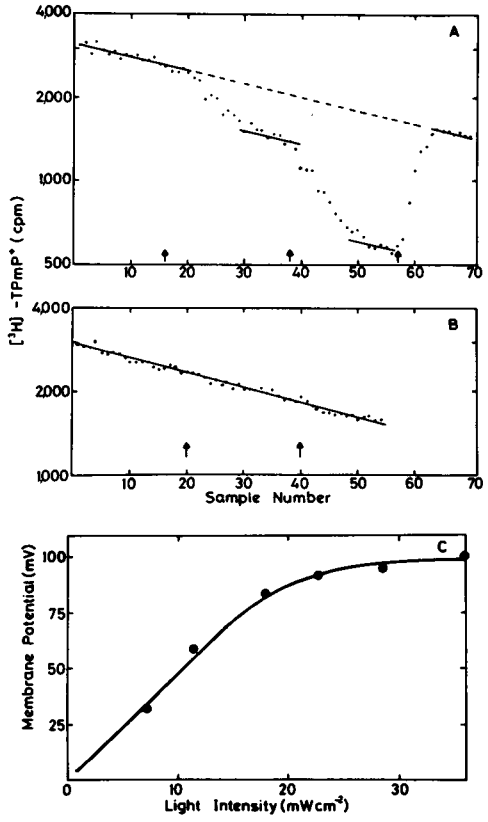

FIGURE 1 Light intensity dependence of the steady state membrane potential in *H. halobium* cell envelope vesicles. $\Delta\Psi$ was measured by flow dialysis of (^{3}H)-TPMP$^+$ uptake at 22°C using vesicles loaded and suspended in 3 M NaCl + 50 mM HEPES (pH 7.6). (*A*) Cell envelope vesicles initially in the dark were illuminated at 11.4 mW cm^{-2} (first arrow), at 28.6 mW cm^{-2} (second arrow), and at 28.6 mW cm^{-2} with 10 μM CCCP added (third arrow). (*B*) A nonvesicular membrane fraction (see text) was illuminated at 36 mW cm^{-2} (first arrow) and then 10 μM CCCP was added (second arrow). (*C*) Light intensity dependence of $\Delta\Psi$ obtained from *A* and similar experiments.

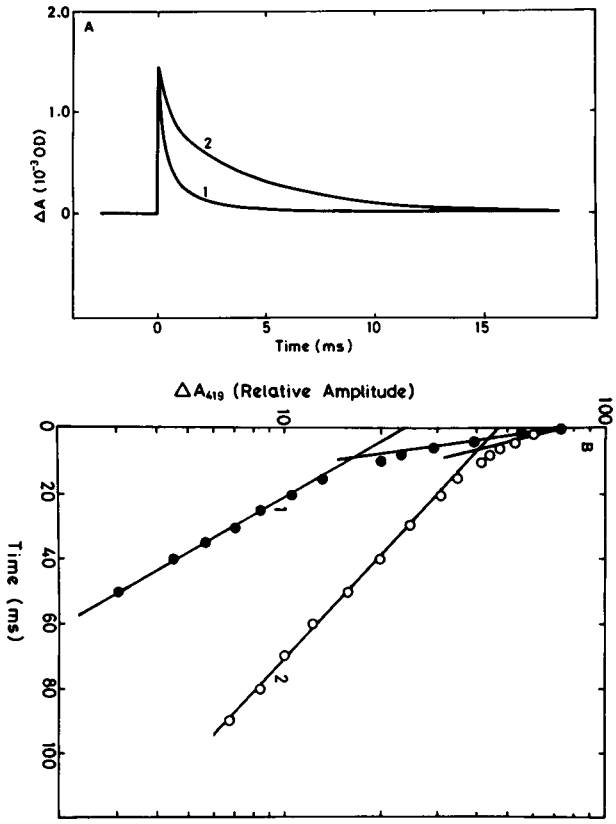

FIGURE 2 Effect of background illumination on the decay kinetics of the M photocycle intermediate measured in cell envelope vesicles. The vesicles were loaded and suspended in 3 M NaCl + 50 mM HEPES (pH 7.6) at 22°C. (*A*) Laser flash-induced absorbance changes monitored at 415 nm (*1*) in the dark and (*2*) with 4 mW cm^{-2} background illumination. (*B*) Semilog plots of the flash-induced absorbance decay at 415 nm (M intermediate) with background illumination (o) 4 mW cm^{-2} and in the dark (•).

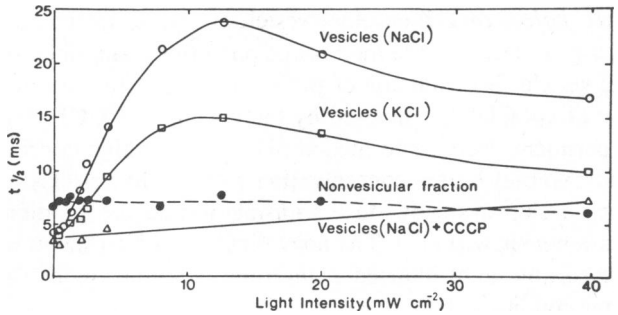

FIGURE 3 Intensity dependence of the M decay half-time on background illumination measured in (○) vesicles in 3 M NaCl, (□) vesicles in 3 M KCl, (△) vesicles in 3 M NaCl with 10μM CCCP added and (●) a nonvesicular membrane fraction in 3 M NaCl. All salt solutions contained 50 mM HEPES (pH 7.6).

vesicles to which CCCP has been added, the $t_{1/2}$ of the M decay is a much flatter function of background light intensity. The 8-25% interface fraction from Ficoll gradient centrifugation which is rich in bR but does not contain any closed vesicles showed no change in its M decay kinetics as a function of background light intensity.

The dependence of $t_{1/2}$ on light intensity shown in Fig. 3 is quite complex because the M decay is multiphasic. The M decay has already been shown to be biphasic under certain conditions in pm sheets (14). In our vesicle preparations, a satisfactory fit required one fast exponential for the rise and two slower exponentials for the decay. Here we shall consider only the decay kinetics. The lifetime of the faster process increases from 3 to 8 ms for light intensities from 0 to 20 mW cm^{-2} (Fig. 4). In the absence of background illumination, this lifetime is close to the decay time of 3 ms observed for the M form in pm sheets. The lifetime of the slower process increases rather sharply with light intensity from 23 to 42 ms and then slowly decreases. The corresponding amplitudes (Fig. 4 *B*) change in opposite directions; the amplitude of the faster process decreases, while that of the slower process increases with increasing background light intensity. The sum of the amplitudes, however, decreases with increasing intensity. This latter effect is discussed below.

We also measured the wavelength dependence of the decay kinetics in the dark and in moderate background light (Fig. 5). The decay curves at all wavelengths were analyzed by curve fitting to a sum of exponentials using a common set of rates that optimized the fit to the entire data set. In the 380–540 nm range two exponentials were required to produce good fits to the decay curves (Fig. 5). The values of the lifetimes are similar to those found at 415 nm. Also, in accordance with the 415-nm data, the amplitude of the faster process is higher in the dark, but lower under illumination. The shapes of all the wavelength dependence curves in the 380–450 nm range resemble each other, and correspond well to the published spectra of the M intermediate (15, 16). However, at longer wavelengths differences occur. The amplitude of the fast process in the

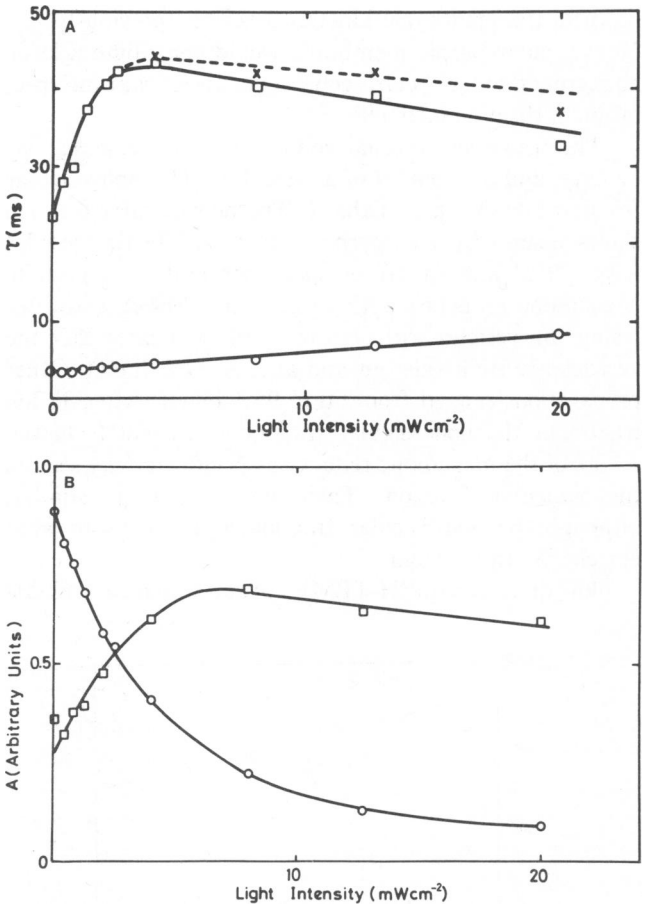

FIGURE 4 Lifetimes and amplitudes of two exponentials fitted to the 415-nm absorbance change data. Experimental conditions as described in Fig. 2. (*A*) Lifetimes (k^{-1}) of the two exponentials vs. background illumination intensity. The dashed line shows the correction for the decrease in bR caused by the background light calculated on the basis of Eq. 11. (*B*) Preexponential (amplitude) factors of the exponentials for the (○) fast and (□) slow processes.

light decreases above 450 nm and there is a small shoulder at 500 nm in the slower component, which is completely missing from the faster one. The relative weight of this peak is higher in the dark.

A plausible interpretation of these two kinetic components is their identification with two distinct processes. Previous modeling of the bR photocycle with two M-like intermediates has been reported (14, 17, 18, 19). We will discuss the results in terms of the two simplest models, where (*a*) two M forms appear sequentially

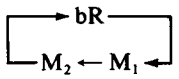

or (*b*) there is a branch at some intermediate X preceding M

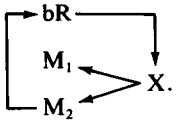

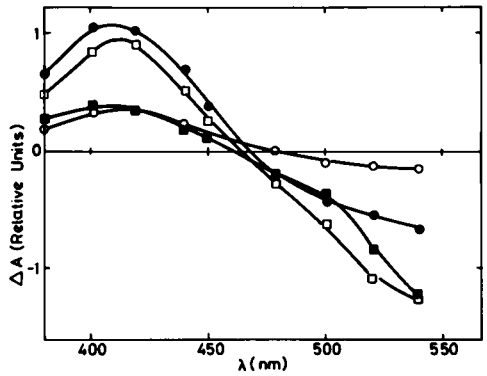

FIGURE 5 Wavelength dependence of the preexponential factors (see Fig. 4 and text) for the (●) fast and (■) slow processes in the dark and for the (○) fast and (□) slow processes at a 4 mW cm^{-2} background illumination intensity.

Note that branching during the decay of M to two subsequent intermediates would give rise to a monophasic decay. Other, more complicated models, which include back reactions between photointermediates, have been proposed (20) and our analysis does not rule out such possibilities. The testing of detailed photocycle models will require data at more wavelengths and faster time scales than presented here (21).

The presence of continuous background illumination has an effect that must be taken into account in the analysis of either model. This illumination decreases the steady state concentration of ground state bR (i.e., via the inhomogeneous term in Eq. 1); this decrease gives rise to the observed decrease in the sum of the decay amplitudes with increasing background light intensity (Fig. 4 *B*). The background light may also modify the decay kinetics, as discussed below in detail (see Eqs. 5 and 11).

Sequential Model

We analyzed a simplified model of the bR photocycle. In this model, the transitions bR → K → L → M are replaced by an infinitely fast single process. This means that the background light causes a continuous rise of M_1, the rate of which is determined by the light intensity (see second term in Eq. 1). Intermediate M_2 is assumed to decay directly to bR. Finally, the laser flash is assumed to instantaneously give rise to an increased concentration of M_1 (i.e. this model does not treat the rise of M_1). Since both the observed decays and the background excitation rate (vide infra) are much slower than the photocycle steps preceding M (20), and since the decay rate of the later intermediate O is similar to that of the slower decaying M component (20, 22), these assumptions are reasonable for discussing the M intermediates. Also, the experiments are performed at pH 7.5 in high salt concentrations, where the contribution of O to the photocycle is decreased because the O intermediate is very pH sensitive as compared with M (22).

For low sample optical densities at 550 nm, the differential equations describing model (*a*) are

$$[\dot{M}_1] = -k_1[M_1] + \sigma\Phi[bR]_0 - [M_1] - [M_2];$$
$$[\dot{M}_2] = k_1[M_1] - k_2[M_2], \quad (1)$$

where $[bR_0]$ is the concentration of bR in the dark, k_i is the rate of decay of M_i, Φ is the intensity of the background illumination, and σ is the product of the absorption cross section of bR at 550 nm and the quantum yield of the bR → M_1 transition. The last term of Eq. 1 describes the effect of background illumination. For a quantum yield of 0.3 (23),

$$\sigma = \frac{6 \times 10^4 M^{-1}cm^{-1}}{6.02 \times 10^{23} mol^{-1}} \ln(10) \times 0.3 \approx 6.9 \times 10^{17} cm^2.$$

With the definitions $m_i = (M_i)/(bR)_0$ and $m'_i = (m_i -$ the steady state value of $m_i)$, the inhomogeneous system of Eq. 1 can be converted to the homogeneous system

$$\dot{m}'_1 = -(k_1 + \sigma\Phi)m'_1 - \sigma\Phi m'_2;$$
$$\dot{m}'_2 = k_1 m'_1 - k_2 m'_2. \quad (2)$$

The initial condition of Eq. 2 is determined by the laser flash intensity. If the extinction coefficients of the two M forms are assumed equal, the measured absorption changes are proportional to $m'_1 + m'_2$.

The linear, homogeneous, first-order system of Eq. 2 can be solved by standard methods (24) to give

$$m'_1(t) + m'_2(t) = A_+ e^{-\lambda_+ t} + A_- e^{-\lambda_- t}, \quad (3)$$

where

$$A_\pm = \frac{\pm m'_1(0)(\lambda_\pm - k_1 - k_2)}{\lambda_+ - \lambda_-}, \quad (4)$$

and

$$\lambda_\pm = \tfrac{1}{2}\{(k_1 + k_2 + \sigma\Phi) \pm [(k_1 + k_2 - \sigma\Phi)^2 - 4k_1k_2]^{1/2}\}. \quad (5)$$

The quantities $A_\pm$ and $\lambda_\pm$ are determined experimentally by fitting the decaying portions of the observed laser-induced transients to a sum of two exponentials. However, there is a constraint on the values of these parameters

$$\frac{-A_-}{A_+} = \frac{\lambda_+ - \sigma\Phi}{\lambda_- - \sigma\Phi}. \quad (6)$$

The left and right-hand sides of Eq. 6 are plotted as a function of background light intensity in Fig. 6. Clearly, they are not equal, as would be predicted from this sequential model. Another important consequence of the structure of the differential system of Eq. 2 is that A_+ and A_- in Eq. 4 have opposite signs (the product A_+A_- is equal to $-C^2k_1k_2$, where C is a constant; since k_1, k_2 are assumed >0, A_+ and A_- must have opposite signs.) Therefore, opposite signs for the A values should be observed if the two M intermediates occur sequentially. Fig. 4 *B* shows that the observed A values have the same sign. Therefore,

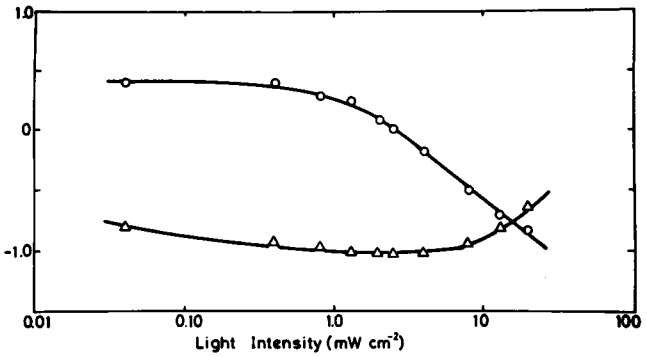

FIGURE 6 Values of (○) $-A_-/A_+$ and (△) $\lambda_+ - \sigma\Phi/\lambda_- - \sigma\Phi$ vs. background illumination intensity calculated from the sequential model (see text).

the sequential model can be rejected by two independent criteria. Note, however, that neither criterion holds generally if the extinction coefficients of the two M-forms are different.

Branching Model

We employ the same simplifications used in the sequential model. The branching takes place at intermediate X, where bR → X is considered a single transition, the rate of which is determined by the excitation rate. Branching is characterized by a branching ratio f, which is the probability that a given molecule in state X will decay to state M_1. If X has decay rates k'_1 and k'_2, and the decays from X to M_1 and M_2 are irreversible, then

$$\frac{f}{1-f} = \frac{k'_1}{k'_2}. \tag{7}$$

The rate constants k'_1 and k'_2 are assumed to be much larger than the excitation rate constant $\sigma\Phi$. Therefore, the effective rates of creation of M_1 and M_2 by the background illumination are $f\sigma\Phi(bR)$ and $(1-f)\sigma\Phi(bR)$, respectively. Moreover, the initial condition for the laser-induced transient is that $m'_1(0)$ and $m'_2(0)$ are in the ratio $f/(1-f)$.

Using the same notation and initial steps as in the sequential model, the branching model analogue of Eq. 2 is

$$\begin{aligned} \dot{m}'_1 &= -(k_1 + \sigma\Phi f)m'_1 - \sigma\Phi f m'_2; \\ \dot{m}'_2 &= -\sigma\Phi(1-f)m'_1 - (k_2 + \sigma\Phi(1-f))m'_2. \end{aligned} \tag{8}$$

This system of equations can be solved by the same methods used to solve Eq. 2. The expected form of the decay of the transient is again given by Eq. 3, except that now

$$\lambda_\pm = \tfrac{1}{2}\{k_1 + k_2 + \sigma\Phi \pm [(k_1 + k_2 + \sigma\Phi)^2 - 4k_1k_2 - 4k_1\sigma\Phi(1-f) - 4k_2\sigma\Phi f]^{1/2}\}, \tag{9}$$

and

$$A_\pm = \frac{\pm A(0)[\lambda_\pm - k_1(1-f) - k_2 f]}{\lambda_+ - \lambda_-}. \tag{10}$$

The addition of the parameter f removes the constraint upon the experimentally measured quantities $A_\pm$ and $\lambda_\pm$. In addition, Eqs. 9 and 10 can be solved for k_1, k_2, and f

$$\begin{aligned} k_1 &= \tfrac{1}{2}[\lambda_+ + \lambda_- - (1-c)\sigma\Phi], \\ k_2 &= \tfrac{1}{2}[\lambda_+ + \lambda_- - (1+c)\sigma\Phi], \\ f &= \frac{1}{2c}\left(\frac{A_+ - A_-}{A_+ + A_-}\frac{\lambda_- - \lambda_+}{\sigma\Phi} + c - 1\right), \end{aligned} \tag{11}$$

where

$$c = \left[\left(\frac{\lambda_- - \lambda_+}{\sigma\Phi}\right)^2 - 2\left(\frac{A_+ - A_-}{A_+ + A_-}\frac{\lambda_- - \lambda_+}{\sigma\Phi}\right) + 1\right]^{1/2}. \tag{12}$$

The first two equations of set 11 describe the corrections needed to arrive at the true M decay rates in the presence of background light. The results of these corrections are shown in Fig. 4 *A*. The only significant correction is to the slower rate at high light intensities. The correction reduces the decrease in the lifetime with increasing intensity. The data presented here are not good enough to unequivocally decide if the residual decrease in Fig. 4 *A* is real. Alternatively, the residual decrease may be due to a photolysis reaction of the O intermediate by the background illumination (20).

The dependence of the branching ratio f on the background light intensity is plotted in Fig. 7. The calculated curve is smooth, saturating, and monotonically decreasing, suggesting a physically relevant relationship between background light intensity and branching ratio. Finally, from Eqs. 9 and 10, the product A_+A_- is equal to $D^2f(1-f)$, where D is a constant. Since $|f| < 1$, A_+ and A_- must have the same sign, in agreement with our observations (Fig. 4 *B*).

DISCUSSION

We have shown that the kinetic parameters of the M decay in energetically closed vesicles are strongly affected by background illumination. This effect is not observed in nonvesicular samples and is markedly reduced in CCCP-treated vesicles. Background illumination generates a protonmotive force across the membrane that controls, or correlates with a process that controls, the photocycle. Because there is no measurable pH gradient under the conditions employed here, the data indicate that the control of the M decay kinetics correlates with the magnitude of $\Delta\Psi$.

The M decay can be satisfactorily fitted by a sum of two exponential components. Their absorption spectra, determined by the preexponential factors, are very similar in the

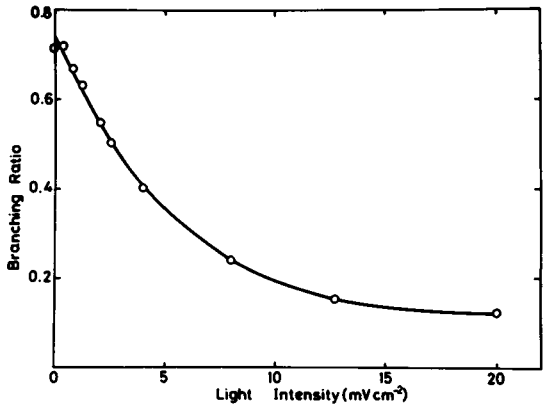

FIGURE 7 Values of the branching ratio (f) vs. background illumination intensity calculated from the branching model (see text).

390–450 nm region and agree with published M spectra. However, we found a definite shoulder at ~500 nm in the spectrum of the slower component. It may be caused by the N intermediate of the photocycle, although its existence is still controversial (15). Detailed analysis of this and the other differences between the components in the 450–550 nm region will require more experimental data.

To explain the two exponentials, we have assumed two spectrally similar M-like forms. Biphasic decay of M has been observed under different conditions and has often been explained by both sequential and branched models. A simple sequential model that assumes no back reactions between photocycle intermediates, however, is not in agreement with our data. Another simple model, which assumes a branching in the cycle before M, is consistent with our results. The branching can take place at the L form or at any previous step. We have calculated the rate constants for the decay of the two M intermediates and their ratio at the branching in the framework of this model and find that these parameters are strongly dependent on the processes that also generate $\Delta\Psi$. Neither model is proposed as a true physical description of the complex bR photocycle.

A change in kinetic parameters reflects a change in the activation energy of the corresponding transition. Keszthelyi and Ormos (25) have shown that every step in the photocycle correlates with charge (probably proton) movement within and across the membrane. Charge movement in an electric field indicates a modification of energy barriers. Assuming a single proton moves a distance d perpendicularly to the membrane during a given transition, the energy barrier is

$$E(\Delta\Psi) = E(0) + \frac{\Delta\Psi}{D} Qd, \qquad (13)$$

where $\Delta\Psi$ is the membrane potential, D is the thickness of the membrane, and Q is the elementary charge. Using the Arrhenius equations, the decay rate constants of M_1 and M_2 are

$$\ln k(\Delta\Psi)_{1,2} = \ln k(0)_{1,2} - \frac{Qd_{1,2}}{DkT}\Delta\Psi. \qquad (14)$$

Plotting $\ln k_{1,2}$ against $\Delta\Psi$, this equation predicts a straight line, the slope of which determines the distance of the proton movements.

Similarly for the branching step (see Eq. 7),

$$\ln \frac{k_1'(\Delta\Psi)}{k_2'(\Delta\Psi)} = \ln \frac{f(\Delta\Psi)}{1 - f(\Delta\Psi)}$$

$$= \ln \frac{f(0)}{1 - f(0)} - \frac{Q(d_1' - d_2')}{DkT}\Delta\Psi. \qquad (15)$$

Fig. 8 shows the logarithm of k_1, k_2, and k_1'/k_2' vs. $\Delta\Psi$. Only the faster rate constant follows a linear dependence. This gives $d/D = 0.25$, which is a reasonable value but slightly less than that measured by Keszthelyi and Ormos using the photoelectric response technique (PERS). From the beginning part of $\ln(k_1'/k_2')$, we measure $(d_2' - d_1')/D = 2.2 > 1$, indicating a total charge movement twice the membrane thickness, which is unreasonable. Even supposing two protons move, this value is too high (25).

This contradiction and the strong nonlinearity of the two curves show that the behaviors of the kinetic parameters are more complex. One can assume that factors other than the membrane potential also affect them. For example, bR-proton pumping may produce local proton concentration differences near the membrane surfaces that are not expressed as a bulk pH gradient. This could give rise to the protonation or deprotonation of specific groups with subsequent alteration of the photocycle reaction mechanism. Another possibility is that the strong electrical field causes conformational changes in the protein, thus changing the barriers. Finally, it is also possible that the fit with two exponentials does not indicate two transitions, but is instead a numerical fit to a process that is really nonexpon-

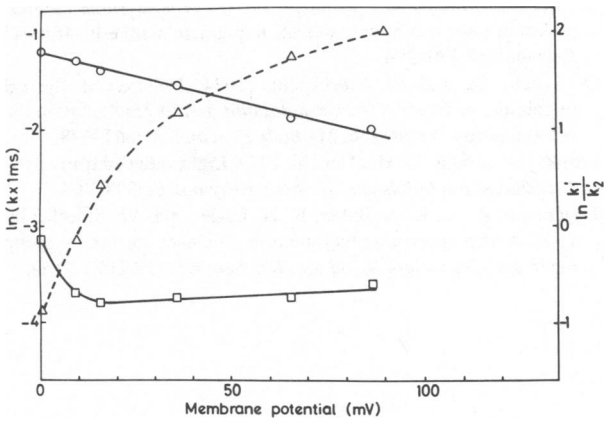

FIGURE 8 Membrane potential dependence of the calculated branching model parameters (○) $\ln k_1$ (fast process), (□) $\ln k_2$ (slow process) and (△) $\ln k_1'/k_2'$. See text for details.

ential. In the case of protein molecules, a single first-order process can result in a nonexponential decay, if the protein can exist in many different conformational states with slightly different activation energies. This leads to a so-called polychromatic reaction. The existence of polychromatic reactions has been shown in other fields of protein research (26, 27). An evaluation of our data in the framework of this theory is in progress.

Thanks are due to Dr. E. Kun for use of the Branson sonicator, Drs. P. Ormos and L. Zimanyi for their help in the interpretation of data, and to Dr. E. Heinz for invaluable discussions concerning the theoretical basis of this work.

This work was supported by the National Science Fountation INT 78-27606 and the National Institutes of Health GM-27057 Program Project grants.

Received for publication 2 March 1983 and in final form 14 November 1983.

REFERENCES

1. Stoeckenius, W., R. H. Lozier, and R. Bogomolni. 1979. Bacteriorhodopsin and the purple membrane of halobacteria. *Biochim. Biophys. Acta.* 505:215–278.
2. Heinz, E. 1980. Electrogenic and electrically silent proton pumps. *In* Hydrogen Ion Transport in Epithelia. I. Schultz, editor. Elsevier/North-Holland Press, Amsterdam. 41–45.
3. Dancshazy, Zs., S. L. Helgerson, and W. Stoeckenius. 1983. Coupling between the bacteriorhodopsin photocycle kinetics and the protonmotive force. I. Single flash measurements in *Halobacterium halobium* cells. *Photobiochem. Photobiophys.* 5:347–357.
4. Dubrovskii, V. T., S. P. Balashov, O. A. Sineshchekov, L. N. Chekulaeva, and F. F. Litvin. 1983. Photoinduced changes in the quantum yields of the photochemical cycle of conversions of bacteriorhodopsin and grans membrane transport of protons into *Halobacterium halobium* cells. *Biochemistry (USSR).* 47: 1036–1046.
5. Watters, F., D. Kuschmitz, and B. Hess. 1982. Coupling of the photocycle and proton current in bacteriorhodopsin: a regulated phenomenon. *Hoppe-Seyler's Z. Physiol. Chem.* 363:5491.
6. Weber, H. J., and R. A. Bogomolni. 1981. P588, a second retinal-containing pigment in *Halobacterium halobium. Photochem. Photobiol.* 33:601–608.
7. Weber, H. J., and R. A. Bogomolni. 1982. The isolation of halobacterium mutant strains with defects in pigment synthesis. *Methods Enzymol.* 88:379–390.
8. Oesterhelt, D., and W. Stoeckenius. 1974. Isolation of the cell membrane of *Halobacterium halobium* and its fractionation into red and purple membrane. *Methods Enzymol.* 31:667–678.
9. Lanyi, J. K., and R. E. MacDonald. 1979. Light-induced transport in *Halobacterium halobium. Methods Enzymol.* 56:398–407.
10. Bogomolni, R. A., R. A. Baker, R. H. Lozier, and W. Stoeckenius. 1980. Action spectrum and quantum efficiency for proton pumping in *Halobacterium halobium. Biochemistry.* 19:2152–2159.
11. Lanyi, J. K. 1972. Studies of the electron transport chain of extremely halophilic bacteria. VII. Solubilization properties of menadione reductase. *J. Biol. Chem.* 247:3001–3007.
12. Bakker, E. P., H. Rottenberg, and S. R. Caplan. 1976. An estimation of the light-induced electrochemical potential difference of protons across the membrane of *Halobacterium halobium. Biochim. Biophys. Acta.* 440:557–572.
13. Lanyi, J. K., S. L. Helgerson, and M. P. Silverman. 1979. Relationship between protonmotive force and potassium ion transport in *Halobacterium halobium* envelope vesicles. *Arch. Biochem. Biophys.* 193:329–339.
14. Korenstein, R., B. Hess, and D. Kuschmitz. 1978. Branching reactions in the photocycle of bacteriorhodopsin. *FEBS (Fed. Eur. Biochem. Soc.) Lett.* 93:266–270.
15. Lozier, R. H., R. A. Bogomolni, and W. Stoeckenius. 1975. Bacteriorhodopsin: A light-driven proton pump in *Halobacterium halobium. Biophys. J.* 15:955–962.
16. Becher, B., F. Tokunaga, and T. G. Ebrey. 1978. Ultraviolet and visible absorption spectra of the purple membrane protein and the photocycle intermediates. *Biochemistry.* 17:2293–2300.
17. Slifkin, M. A., and S. R. Caplan. 1975. Modulation excitation spectrophotometry of purple membrane of *Halobacterium halobium. Nature (Lond.).* 253:56–58.
18. Lozier, R. H., W. Niederberger, R. A. Bogomolni, S. B. Hwang, and W. Stoeckenius. 1976. Kinetics and stoichiometry of light-induced proton release and uptake from purple membrane fragments, *Halobacterium halobium* cell envelopes, and phospholipid vesicles containing oriented purple membrane. *Biochim. Biophys. Acta.* 440:545–556.
19. Ohno, K., Y. Takeuchi, and M. Yoshida. 1981. On the two forms of intermediate M of bacteriorhodopsin. *Photochem. Photobiol.* 33:573–578.
20. Lozier, R. H., W. Niederberger, M. Ottolenghi, G. Sivorinovsky, and W. Stoeckenius. 1978. On the photocycles of light- and dark-adapted bacteriorhodopsin. *In* Energetics and Structure of Halophilic Microorganisms. S. R. Caplan and M. Ginzburg, editors. Elsevier/North-Holland Biomedical Press, New York. 123–141.
21. Nagle, J. F., L. A. Parodi, and R. H. Lozier. 1982. Procedure for testing kinetic models of the photocycle of bacteriorhodopsin. *Biophys. J.* 38:161–174.
22. Lozier, R. H., and W. Niederberger. 1977. The photochemical cycle of bacteriorhodopsin. *Fed. Proc.* 36:1805–1809.
23. Becher, B., and T. G. Ebrey. 1977. The quantum efficiency for the photochemical conversion of the purple membrane protein. *Biophys. J.* 17:185–191.
24. Sanchez, D. A. 1968. The Linear Equation with Constant Coefficients. *In* Ordinary Differential Equations and Stability Theory. An Introduction. W. H. Freeman and Co., San Francisco/London. 58–65.
25. Keszthelyi, L., and P. Ormos. 1980. Electrical signals associated with the photocycle of bacteriorhodopsin. *FEBS (Fed. Eur. Biochem. Soc.) Lett.* 109:189–193.
26. Goldanskii, V. I. 1979. Facts and hypotheses of molecular chemical tunnelling. *Nature (Lond.).* 279:109–115.
27. Austin, R. H., K. W. Beeson, L. Eisenstein, H. Frauenfelder, and I. C. Gunsalus. 1975. Dynamics of ligand binding to myoglobin. *Biochemistry.* 14:5355–5373.